Empirically estimated electron lifetimes in the Earth's radiation belts: 1. Observations

S. G. Claudepierre[1,2], Q. Ma[2,3], J. Bortnik[2], T. P. O'Brien[1], J. F. Fennell[1], and J. B. Blake[1]

[1]Space Sciences Department, The Aerospace Corporation, El Segundo, California, USA
[2]Department of Atmospheric and Oceanic Sciences, UCLA, Los Angeles, California, USA
[3]Center for Space Physics, Boston University, Boston, Massachusetts, USA

Key Points:

- A large database of radiation belt electron decay timescales is calculated from Van Allen Probes MagEIS measurements
- Long lifetimes are found in the inner zone ($\sim$100 days); shorter lifetimes are found in the outer zone and slot region ($\sim$1-20 days)
- The decay timescales generally agree well with prior estimates; some differences exist and may be due to instrumental effects

Corresponding author: S. G. Claudepierre, sethclaudepierre@gmail.com

Abstract

We use measurements from NASA's Van Allen Probes to calculate the decay time constants for electrons over a wide range of energies (30 keV - 4 MeV) and L values ($L =$ 1.3 - 6.0) in the Earth's radiation belts. Using an automated routine to identify flux decay events, we construct a large database of lifetimes for near-equatorially-mirroring electrons over a 5-year interval. We find long lifetimes ($\sim$100 days) in the inner zone that are largely independent of energy, contrasted with shorter, energy-dependent lifetimes ($\sim$1-20 days) in the slot region and outer zone. We compare our lifetime calculations with prior empirical estimates and find good quantitative agreement. The comparisons suggest that some prior estimates may overestimate electron lifetimes between $L \approx$ 2.5-4.5 due to instrumental effects and/or background contamination. Previously reported two-stage decays are explicitly demonstrated to be a consequence of using integral fluxes.

Plain Language Summary

The Earth is surrounded by two invisible, donut-shaped belts of charged particle radiation (think electrons and protons) called the Van Allen belts. The particles in these belts orbit rapidly around the Earth in the same region where spacecraft fly, like GPS and weather satellites. Since the particles in the belts can damage satellites, we need to understand what specific processes make the intensity of the belts go up and down. Knowing which processes are important for changing the belt intensity helps us build better computer models that can be used to predict the future state of the belts (much like weather prediction models). This letter, along with a companion letter, examines the processes that make the belt intensity go down. We use both spacecraft observations and theoretical calculations to determine which of these "loss" processes are the most important. One particularly interesting result is that we show that high-powered radio wave transmitters that are used to communicate with submarines can enhance the loss of particles from the inner belt.

1 Introduction

The Earth's electron radiation belts rarely, if ever, reach a state of equilibrium and exist in a constant state of flux, the result of competition between various source and loss processes. During highly dynamic intervals, such as geomagnetic storms, both the source and loss processes generally operate on fast timescales ($\sim$1 day or less). Outside of storm times, the balance of longer-timescale processes (e.g., pitch angle and radial diffusion) determines the overall configuration of the belts, which are often observed to decay exponentially following enhancements. Many authors have calculated these electron decay time constants, or "lifetimes," from observations at various energies and locations throughout the belts to help elucidate the relevant physics (e.g., Roberts, 1969; Vampola, 1971; West et al., 1981; Albert, 2000; Seki et al., 2005; Meredith et al., 2006; Baker et al., 2007; Meredith et al., 2009; Benck et al., 2010; Su et al., 2012; Fennell et al., 2012; Ripoll et al., 2015). Such lifetime estimates are useful for radiation belt modeling, whereby the complexity of the problem can be reduced by incorporating all of the loss processes and loss physics into a single model parameter. Accurate calculations of electron lifetimes are also important for quantitative assessments of the radiation hazards posed to spacecraft, particularly in the inner zone where relativistic electrons appear sporadically and exhibit long lifetimes. This manuscript seeks to obtain accurate estimates of these lifetimes from observations and compare them with prior estimates. A companion paper uses the lifetime estimates to constrain and inform our understanding of the relevant physical processes that contribute to the loss of electrons from the radiation belts.

2 Data and Methods

The primary data used in this work are measurements from the Magnetic Electron Ion Spectrometer (MagEIS; Blake et al. (2013)) sensors aboard NASA's Van Allen Probes (Mauk et al., 2013). The twin Van Allen Probes, launched in August 2012, make high-resolution particle, field, and wave measurements throughout the radiation belt region, nominally $L = 1$ - 6. The MagEIS electron spectrometers measure the angular distribution over the spacecraft spin period ($\sim$11 s) for electrons in the energy range $\sim$30 keV to $\sim$4 MeV. The electron fluxes are presented here as daily averages in fixed L bins (0.1L-width) with McIlwain L obtained from the Olson and Pfitzer (1977) quiet model. The measurements are extracted near the magnetic equator when $B/B_{eq} \leq 1.1$, where B/B_{eq} is the ratio of the magnetic field strength at the spacecraft to that at the magnetic equator (both obtained from the model). The fluxes are averaged between 80° and 100° local pitch angle which, for this B/B_{eq} range, corresponds to equatorial pitch angles between 70° and 110°. Background corrected data (Claudepierre et al., 2015) are used exclusively, where the modified technique of Claudepierre et al. (2019) is employed. We present data from Probe B over the 5 year interval from 2013 April 01 through 2018 March 31 and note that the specific data used are the same as in Claudepierre et al. (2019), which were provided as Supporting Information in that manuscript.

An automated algorithm has been developed to identify exponential decays and calculate the e-folding times of the decays from the MagEIS electron measurements. This algorithm, which is described in greater detail in the Supporting Information, is based on the technique of Benck et al. (2010), which was in turn adapted from that of Meredith et al. (2006). The algorithm is designed to estimate decay times over time intervals where the fluxes are decreasing for at least 5 days. The flux time series are fit with an exponential function, $J(t) = J_0 \exp(-t/\tau)$, using two goodness-of-fit parameters to ensure high-quality fits, the linear correlation coefficient and the percent error between the fit and the flux. The fits are obtained at all $L = 1-6$ and we do not sort the decay timescales with respect to the plasmapause location, primarily because none of the prior works with which we compare have done so. In addition, since we obtain fits in fixed L bins, it is difficult to assign an "inside" or "outside" of the plasmasphere designation to an individual decay event, since the plasmapause could move across the fixed L bin during the decay interval. Figure 1a provides an example of the application of the automated procedure at $L = 4.65$ and 467 keV energy.

3 Results

Figure 1 presents statistical results from the decay timescale database obtained. Panel (b) shows the mean decay timescale, or "lifetime," in each L and energy bin. Throughout this work, we use the terms decay timescale and lifetime interchangeably, noting that a more appropriate terminology is "effective" or "apparent" lifetime (e.g., Cunningham et al., 2018). The particle lifetime is an aggregate quantity that may include effects due to a number of different loss mechanisms, such as de-energization due to nonlinear effects, and also tries to capture the lifetimes of a number of modes of the distribution simultaneously. Moreover, the calculated lifetimes could potentially be influenced by a source (e.g., inward radial transport from higher L) and thus may not always be representative of the true, underlying decay timescale. Thus, our calculated decay times represent upper bounds; the true decay times could be lower than those calculated if there are also source processes acting during the decay interval. It is a difficult task to exclude any inward transport or other source processes that may occur simultaneously with the decay, and we have not attempted to do so here. We emphasize that magnetopause shadowing events are effectively excluded from our database by the criteria above that the decay interval must be 5 days or longer. We have not attempted to remove very rapid local loss processes (e.g., microbursts) from the database, which will be smoothed out through the use of daily-averaged fluxes.
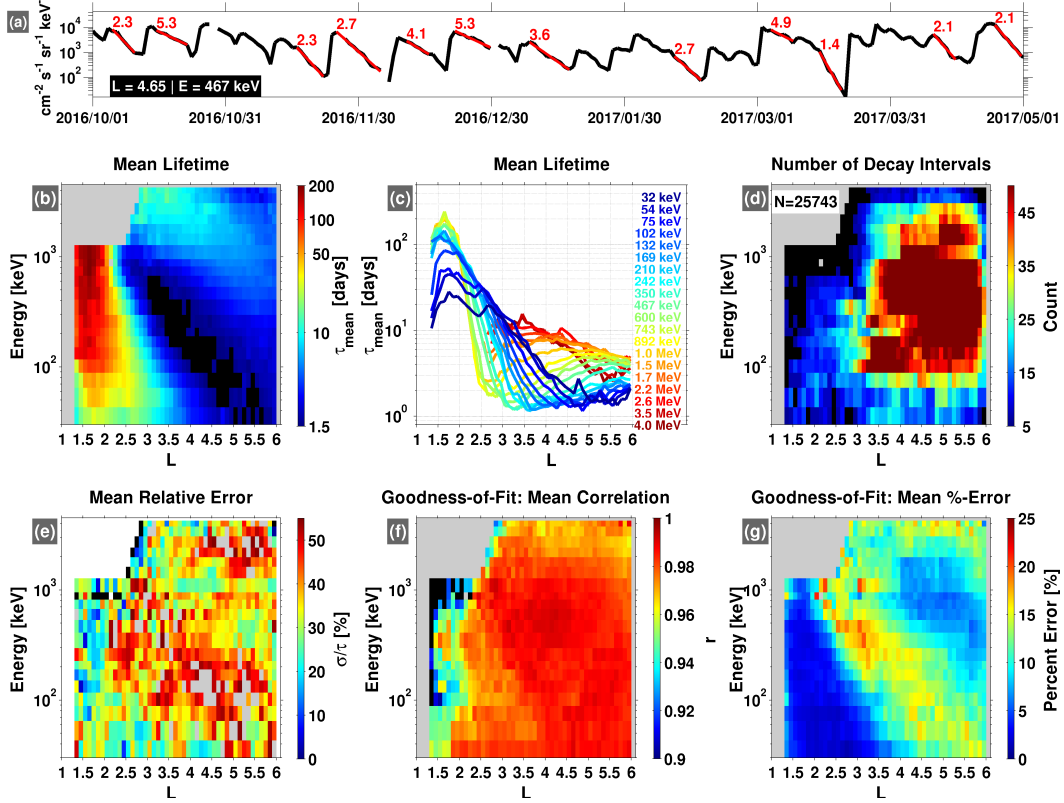
Figure 1. Summary of the decay timescales obtained from the automated algorithm. **(a)** Daily-averaged, differential flux at $L = 4.65$ for 467 keV electrons. Exponential decays identified by the automated algorithm are highlighted in red with the calculated decay (e-folding) times indicated, in days. **(b)** Mean lifetimes calculated in each energy and L bin (0.1L-width). **(c)** Same as panel (b) but here displayed in a line plot format. **(d)** The number of decay intervals identified in each energy and L bin, with the total number in all bins indicated (N). **(e)** The mean relative error (standard deviation divided by the mean) in each energy and L bin (note that grey color in this panel indicates a value above the maximum of the color scale). **(f)-(g)** Goodness-of-fit metrics in each energy and L bin, displaying the mean linear correlation coefficient (r) and the mean percent error between the exponential fit and the flux. In all of the color panels, a black color indicates a value below the indicated color scale.

Returning to Figure 1, we note that the fits are not constructed at $L < 1.3$ due the fact that the fluxes are noisy and subject to considerable orbital effects in this region, from which generally poor results are obtained. In addition, fits are not performed at $L > 6$ due the large variability in the fluxes and the spatial coverage of the Van Allen Probes, which do not sample this region uniformly in time. The region of no data at high energy and low L in panel (b) is due to the fact that there have not been injections of >1.5 MeV electrons into the inner zone at detectable levels during the Van Allen Probes era (Fennell et al., 2015; Claudepierre et al., 2019). Panel (c) shows the same data as panel (b), but presented in line plot format with each energy channel represented by a different color.

The profiles in panels (b) and (c) show that long electron lifetimes ($\tau > 100$ d) are generally observed in the inner zone ($L < 2.5$) above 100 keV and below 1 MeV. In this energy range, the lifetimes peak near $L = 1.7$, are largely independent of en-

ergy, and exhibit steep gradients on either side of the peak where the lifetime changes by $\sim$100 d in approximately one L shell ($d\tau/dL$ not shown here). Moving outward in L, the lifetimes in this energy range then decrease rapidly toward the slot region, which can be identified in panel (b) as the deep blue and black region between $L = 3 - 5$. Here, the lifetimes are on the order of 1-2 d, beyond which they increase slightly towards the outer region near $L = 6$. At energies greater than 1 MeV, the lifetime profiles show a somewhat different character, with less radial dependence and values in the 5-10 d range throughout the outer zone. As we detail in the companion paper, the general structure of the lifetime profiles as a function of energy and L is consistent with quasilinear pitch angle diffusion by various scattering mechanisms (e.g., Coulomb, hiss, EMIC, VLF transmitter).

Panels (d)-(g) in Figure 1 display several parameters related to the statistical database and the automated algorithm. Panel (d) shows the total number of decay intervals identified in each (L,E)-bin, where the color scale saturates at 50 events. We see that the statistics are generally good at $L > 3.5$ and for energies between 100 keV and 1 MeV, with fewer events in the inner zone and in the outer zone at higher energy. Panel (e) shows the mean relative error, which is defined as the standard deviation divided by the mean lifetime, expressed as a percentage. For example, in a given (L,E)-bin, if the mean lifetime is 10 d and the standard deviation is 1 d, then the mean relative error is 10%. We see that the mean relative error is generally less than 50%, i.e., that the lifetimes inferred from the measurements vary by a factor of $\sim$2 around the mean, which is consistent with similar prior calculations (e.g., Benck et al., 2010; Baker et al., 2007). Panels (f) and (g) show the two goodness-of-fit criteria used in the automated search (see Supporting Information), displaying high correlations and low errors between the fits and the fluxes throughout most of the region. As noted above and in the Supporting Information, the criteria on the quality of the fits must be relaxed in the inner zone and at the highest energies to boost statistics. The largest percent errors are observed in the slot region, due to the low flux levels often found there, which leads to enhanced Poisson (counting statistics) noise relative to other regions where higher flux levels are typically observed.

4 Discussion

Figure 2 compares the mean lifetimes from MagEIS with those obtained in previous works using similar techniques. In each panel, the MagEIS mean lifetime is shown in grey as a function of L at a fixed energy. Previously published lifetime estimates are displayed using different colors when those estimates are available in a comparable energy channel to the MagEIS channel. For example, panel (c) shows an L profile of the mean lifetime estimate from MagEIS, along with 4 additional L profiles where the reference and energy channel are provided in the figure legend. The Supporting Information gives further details for each of the previously published estimates (spacecraft, instrument, orbit, etc.). Overall, we find good quantitative agreement between the MagEIS lifetime estimates obtained here and those from past works, namely the long lifetimes in the inner zone and the steep negative gradients into the slot region. Some discrepancies are noted, in particular that the MagEIS estimates tend to be slightly lower than the others. These are discussed in greater detail in the next sections.

4.1 Comparisons with Prior Estimates at Low Energy (50 - 250 keV)

At energies between 50 and 250 keV, the comparisons with the prior empirical estimates shown in Figure 2(a)-(c) exhibit some quantitative disagreement with the MagEIS estimates. For example, the estimates from Su et al. (2012) are typically a factor of $\sim$2 of greater than the MagEIS calculations, and exceed the 1σ error bar on the MagEIS estimates. We note, however, that these differences are at the highest Ls and lowest energies, where the MagEIS uncertainties are the largest (e.g., Figure 1, panels (d), (e) and
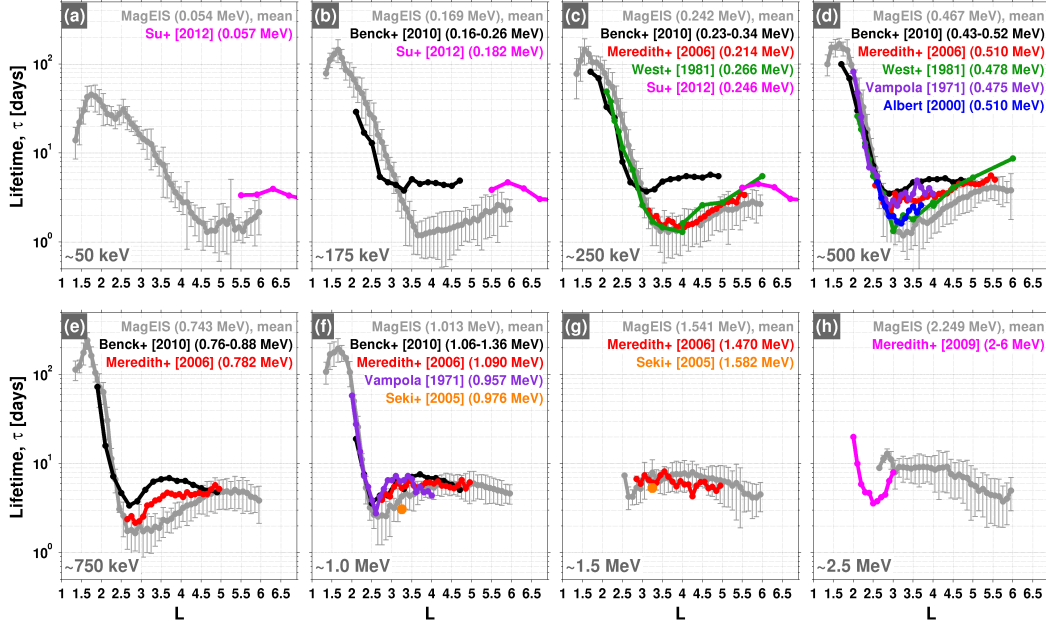
Figure 2. **(a)-(h)** Comparison of the mean lifetimes obtained from MagEIS (grey) with several previously published estimates (color) at 8 fixed energies spanning ~50 keV to ~2.5 MeV. The error bars on the MagEIS lifetimes are one standard deviation on the mean.

(g)). More noteworthy are the differences between the Benck et al. (2010) estimates and the others available for comparison. At 250 keV (panel (c)) above $L \approx 3$, the Benck et al. (2010) estimates are noticeably out of family with the other estimates presented. The Benck et al. (2010) estimates are also higher than MagEIS at all other energies available for comparison, 160-1360 keV (not shown here). Some of these discrepancies between the Benck et al. (2010) estimates and the others may be due to instrumental effects in the DEMETER/IDP measurements that were used (note that SAC-C/ICARE measurements were also used in Benck et al. (2010)). In particular, Selesnick et al. (2019) show that lower energy electrons reported by DEMETER/IDP may actually be measurements of higher energy electrons, due to the instrumental effects of pileup and deadtime. If higher energy electrons (e.g., 1 MeV) are influencing the DEMETER/IDP measurements at lower energy, this could possibly explain the high lifetime estimates, since higher energy electrons have longer lifetimes in general (e.g., Figure 1). Contamination from penetrating high-energy electrons and/or bremsstrahlung may also contribute, as described below.

4.2 Comparisons with Prior Estimates at High Energy (0.5 - 4 MeV)

The comparisons with previous estimates shown in Figure 2 at energies >500 keV (panels (d)-(h)) generally show good quantitative agreement. The steep negative gradients in the lifetimes from the inner zone into the slot region are quantitatively consistent across all energies for all of the estimates, with respect to both the slope and the overall magnitude. However, between $L \approx 2.5-4.5$ some differences are noted between the MagEIS estimates and some of the prior works. For example, at 750 keV (panel (e)) we see that both the Benck et al. (2010) and the Meredith et al. (2006) estimates are higher than the MagEIS lifetimes, exceeding the 1σ error bars on MagEIS. In addition, the shape of the L profiles are different, with the Benck et al. (2010) and Meredith et al. (2006) lifetimes displaying a local maximum near $L \sim 3.5$, whereas the MagEIS lifetimes are increasing with L through this region. We now consider the possibility that

some of these earlier estimates may be influenced by high-energy electron contamination in this region.

Bremsstrahlung x-rays are produced when high energy (e.g., multi-MeV) electrons interact with the spacecraft and instrument materials. These x-rays can register as counts in space-based detectors that are designed to measure energetic particles (e.g., silicon solid state detectors). The MagEIS instrument was designed so that background contamination from bremsstrahlung x-rays (and other sources) could be quantified and removed from the measurements, providing a highly robust measure of foreground electrons. We exploit this capability to examine how high-energy electron contamination may influence lifetime calculations like those presented here.

Figure 3a shows time series of MagEIS electron flux measurements at $L = 3.25$ over the 100 keV to 4 MeV energy range. Both background-corrected and uncorrected profiles are shown. During this time interval, we note that there are two strong enhancements of multi-MeV (2.5 - 4.0 MeV) electrons, one in March 2015 and another in June 2015. Following these enhancements, the electrons at these energies decay slowly with a decay timescale on the order of 10 d. Note the influence that contamination from these multi-MeV electrons has on the uncorrected flux profiles at lower energy. For example at 467 keV, during the time intervals highlighted with grey shading, the background-corrected data reveal that the true dynamics are not that of steady, exponential decays, as is suggested by the uncorrected data. The bremsstrahlung contamination in the uncorrected data produces flux profiles that appear to decay exponentially, but this is simply a manifestation of the decay timescales of the multi-MeV electrons that produce the bremsstrahlung. A similar effect is seen in the other energy channels between 350 keV and 743 keV.

We have preformed an identical statistical analysis of electron lifetimes as described above (e.g., Section 2), but now using the uncorrected MagEIS data. Figure 3b shows the results, where four of the same panels from Figure 2 are shown, but which now also include the calculations for the uncorrected MagEIS data. The effect that the bremsstrahlung contamination described above has on the lifetime calculations is clear. For example, between $L \sim 3\text{-}5$, bremsstrahlung contamination artificially increases the lifetime estimates obtained from the uncorrected MagEIS data, relative to the corrected data. This suggests that some prior lifetime estimates may be influenced by high-energy electron contamination in this region. Specifically, note that the lifetimes obtained from the uncorrected MagEIS data are closer to the values obtained in prior works shown, in terms of both shape and magnitude. We note that this bremsstrahlung contamination interpretation is consistent with our knowledge of the MEA sensor on CRRES, which was used in the Meredith et al. (2006) study. CRRES/MEA shares a design heritage with MagEIS, employing a similar measurement technique, albeit with thicker detectors that are more susceptible to bremsstrahlung contamination than those used in MagEIS. Unfortunately, the telemetry requirements on the CRRES mission precluded downlinking the necessary data to perform background corrections on the MEA measurements. The results presented suggest that the (Benck et al., 2010) estimates may similarly be contaminated by high-energy electrons, including the pileup and deadtime effects noted above.

There are a number of other factors that could lead to the discrepancies found between the MagEIS estimates and those obtained in prior works, such as differences in the techniques used to identify decay intervals and calculate lifetimes, orbital differences, solar cycle differences, and/or differences in the portions of the pitch angle distributions from which the lifetime estimates are made. Such differences have been noted by previous authors conducting similar analyses (e.g., Ripoll et al., 2015). These are not explored further in any detail here however, as we find the overall agreement between the prior estimates and those obtained from MagEIS to be quite good and argue that the remaining differences are likely instrumental in nature. The fact that the majority of the discrepancies lie in a fixed L region ($L = 3$ - 5) also hints that high-energy electron con-
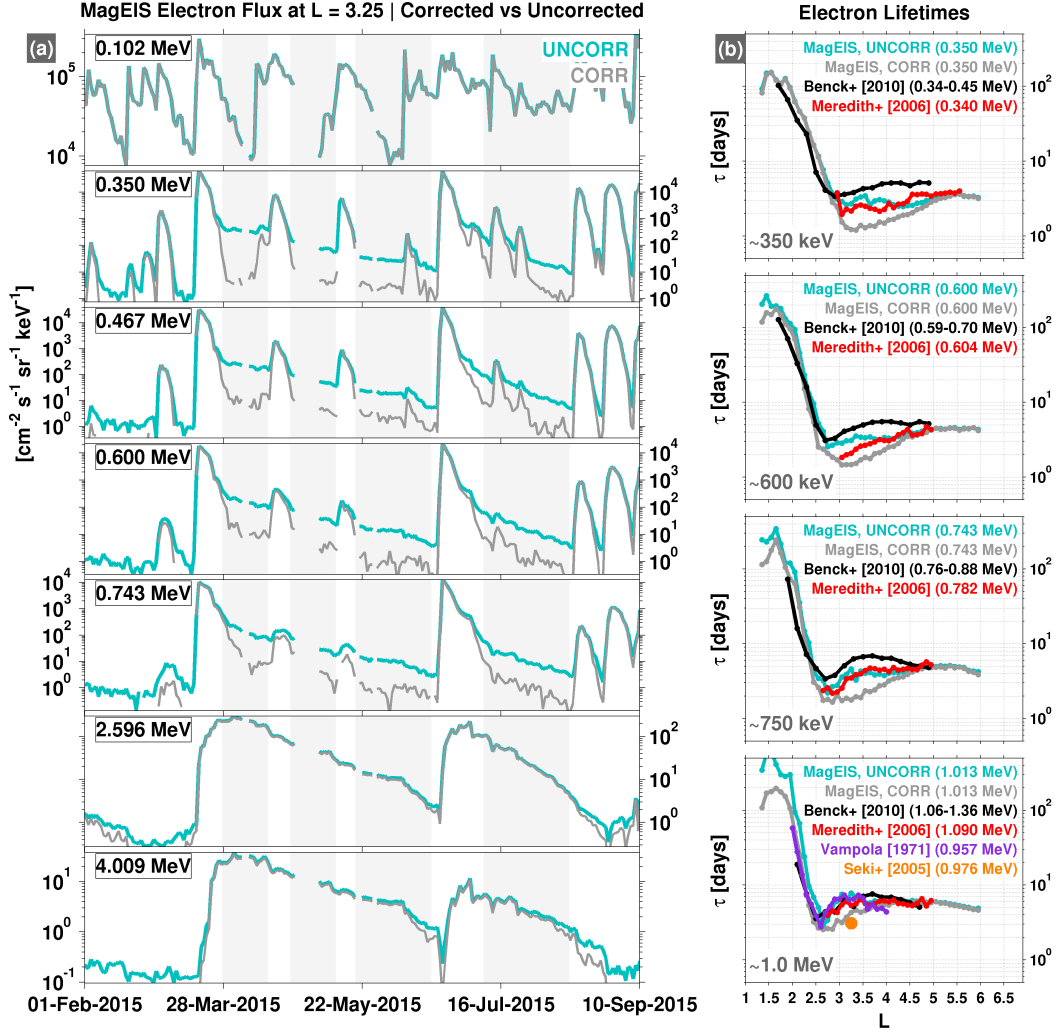
Figure 3. **(a)** A comparison of uncorrected (UNCORR) and background-corrected (CORR) MagEIS electron flux at $L = 3.25$ for the indicated energy channels. Four time intervals are highlighted (grey shaded regions) as times during which bremsstrahlung from multi-MeV electrons contaminates the uncorrected fluxes (most notably between 350 and 743 keV). **(b)** A comparison of lifetimes obtained from both the uncorrected and background-corrected MagEIS electron fluxes, along with several previous empirical estimates.

tamination may be responsible, as one would expect the other potential factors to be systematic across all L.

4.3 Integral Flux Measurements and Two-Stage Decays

As a final application of the capabilities and techniques presented here, we demonstrate the importance of carefully distinguishing between decay rates obtained from differential vs integral fluxes. Several past empirical lifetime estimates have been made using measurements from integral sensors (e.g., those that measure the flux above some threshold energy), rather than the differential fluxes used here, most notably those made following high-altitude nuclear detonations in the late 1950s and early 1960s (e.g., Roberts,

1969, and references therein). As noted by Fennell et al. (2012), electron flux decays observed by integral sensors often exhibit a two-timescale or "two-stage" decay, where a rapid initial decay ($\tau \sim 1$ d) is followed by a more gradual, slower decay ($\tau \sim 20$ d). Ripoll et al. (2015) argued that such observations are the consequence of the wide energy response of integral sensors combined with the wide range of decay timescales as a function of energy at a given L (e.g., Figure 1). We explicitly corroborate this assertion by exploiting the high energy resolution afforded by the MagEIS sensor, in conjunction with the techniques presented above.

Figure 4 compares MagEIS integral fluxes (>0.5 MeV) in panel (a) with differential fluxes in panel (b) from the same energy range (0.5 - 4 MeV), at $L = 2.85$. Note that in Figure 1, the decay timescales at this L vary widely in this energy range, from $\sim$1 d at the lower energies to $\sim$10-20 d at the higher energies. In Figure 4a, we see that the integral fluxes are characterized by a two-stage decay: a rapid, initial decay, followed by a slower decay as time progresses. The differential fluxes in panel (b) reveal that the rapid initial decay in the integral flux is strongly influenced by the fluxes at the lower energy end of the integral channel ($\sim$0.5 MeV) while the second, slower stage of the decay is dominated by the higher energy fluxes, which decay much more slowly than the lower energy fluxes. Thus, we urge caution when interpreting decay timescales obtained from integral channels, or even wide differential channels, since they can mix energy-dependent decay rates, which we have demonstrated are a strong function of energy at a given L. In the companion paper, we show that the energy-dependent decay rates at a given L can be the result of multiple scattering mechanisms operating simultaneously (e.g., hiss wave scattering at low energy and EMIC wave scattering at high energy).
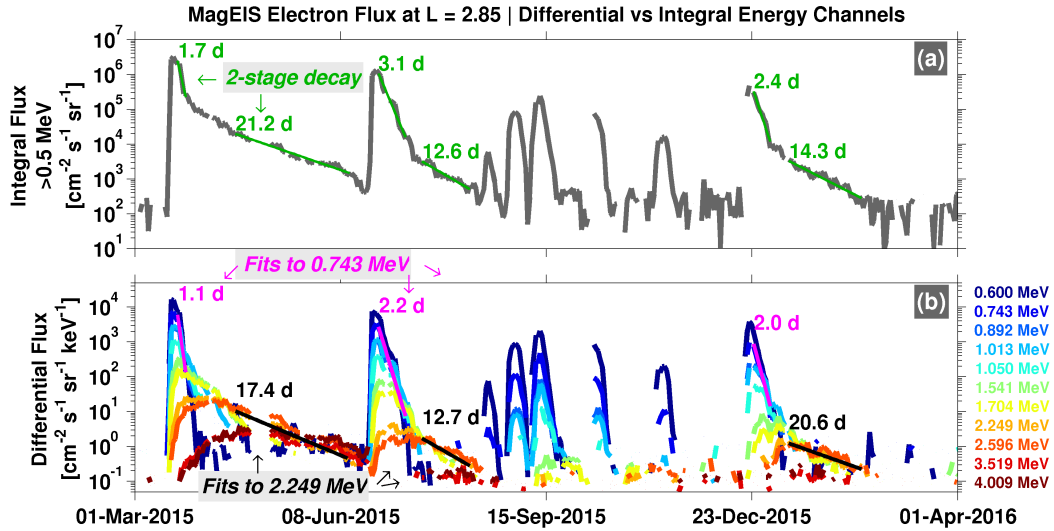

Figure 4. **(a)** MagEIS integral flux (>0.5 MeV) at $L = 2.85$ over a 1 year interval. Note the three instances of two-stage decays (green), where an initial rapid decay ($\tau \approx 1.7$ - 3.1 days) is followed by a more gradual decay ($\tau \approx 13$ - 21 days). **(b)** MagEIS differential flux demonstrating that the two-stage decays in the integral flux are due to energy-dependent decay timescales.

5 Summary

We provide a comprehensive, long-term (5 year) database of energetic and relativistic electron decay timescales observed throughout the radiation belt region. This is the

first such database obtained in a near-equatorial orbit from a single sensor with high-angular and energy resolution and quantifiable background rejection. We find that the decay timescales obtained from MagEIS are largely consistent with previously-obtained empirical estimates, namely long lifetimes in the inner zone, short lifetimes in the slot region, and energy dependent lifetimes in the outer zone indicative of different loss mechanisms. We use the techniques presented to demonstrate that some prior estimates may be influenced by background contamination and that previously reported two-stage decays are likely due to the use of wide energy (integral) flux measurements. A companion paper utilizes this database further to explore the physical mechanisms responsible for the observed decay timescales, which ultimately produce the quiet time structure of the radiation belts.

Acknowledgments

References

Albert, J. M. (2000, Jan). Pitch Angle Diffusion as Seen by CRRES. *Adv. Space Res.*, *25*(12), 2343-2346. doi: 10.1016/S0273-1177(99)00520-7

Baker, D. N., Kanekal, S. G., Horne, R. B., Meredith, N. P., & Glauert, S. A. (2007, Oct). Low-altitude measurements of 2-6 MeV electron trapping lifetimes at 1.5 ≤ L ≤ 2.5. *Geophys. Res. Lett.*, *34*(20), L20110. doi: 10.1029/2007GL031007

Benck, S., Mazzino, L., Cyamukungu, M., Cabrera, J., & Pierrard, V. (2010, Mar). Low altitude energetic electron lifetimes after enhanced magnetic activity as deduced from SAC-C and DEMETER data. *Ann. Geophys.*, *28*(3), 849-859. doi: 10.5194/angeo-28-849-2010

Blake, J. B., Carranza, P. A., Claudepierre, S. G., Clemmons, J. H., Crain, W. R., Dotan, Y., ... Zakrzewski, M. P. (2013, November). The Magnetic Electron Ion Spectrometer (MagEIS) Instruments Aboard the Radiation Belt Storm Probes (RBSP) Spacecraft. *Space Sci. Rev.*, *179*, 383-421. doi: 10.1007/s11214-013-9991-8

Claudepierre, S. G., O'Brien, T. P., Blake, J. B., Fennell, J. F., Roeder, J. L., Clemmons, J. H., ... Larsen, B. A. (2015, July). A background correction algorithm for Van Allen Probes MagEIS electron flux measurements. *J. Geophys. Res.*, *120*, 5703-5727. doi: 10.1002/2015JA021171

Claudepierre, S. G., O'Brien, T. P., Looper, M. D., Blake, J. B., Fennell, J. F., Roeder, J. L., ... Spence, H. E. (2019, February). A Revised Look at Relativistic Electrons in the Earth's Inner Radiation Zone and Slot Region. *J. Geophys. Res.*, *124*, 934-951. doi: 10.1029/2018JA026349

Cunningham, G. S., Loridan, V., Ripoll, J.-F., & Schulz, M. (2018, April). Neoclassical Diffusion of Radiation-Belt Electrons Across Very Low L-Shells. *J. Geophys. Res.*, *123*, 2884-2901. doi: 10.1002/2017JA024931

Fennell, J. F., Claudepierre, S. G., Blake, J. B., O'Brien, T. P., Clemmons, J. H., Baker, D. N., ... Reeves, G. D. (2015, March). Van Allen Probes show that

the inner radiation zone contains no MeV electrons: ECT/MagEIS data. *Geophys. Res. Lett.*, *42*, 1283-1289. doi: 10.1002/2014GL062874

Fennell, J. F., Kanekal, S. G., & Roeder, J. L. (2012). Storm responses of radiation belts during solar cycle 23: HEO satellite observations. In D. Summers, I. R. Mann, D. N. Baker, and M. Schulz (Ed.), *Dynamics of the earth's radiation belts and inner magnetosphere* (Vol. 199). Washington, D.C.: American Geophysical Union. doi: 10.1029/2012GM001356

Mauk, B. H., Fox, N. J., Kanekal, S. G., Kessel, R. L., Sibeck, D. G., & Ukhorskiy, A. (2013, November). Science Objectives and Rationale for the Radiation Belt Storm Probes Mission. *Space Sci. Rev.*, *179*, 3-27. doi: 10.1007/s11214-012-9908-y

Meredith, N. P., Horne, R. B., Glauert, S. A., Baker, D. N., Kanekal, S. G., & Albert, J. M. (2009, Mar). Relativistic electron loss timescales in the slot region. *J. Geophys. Res.*, *114*(A3), A03222. doi: 10.1029/2008JA013889

Meredith, N. P., Horne, R. B., Glauert, S. A., Thorne, R. M., Summers, D., Albert, J. M., & Anderson, R. R. (2006, May). Energetic outer zone electron loss timescales during low geomagnetic activity. *J. Geophys. Res.*, *111*(A5), A05212. doi: 10.1029/2005JA011516

Olson, W. P., & Pfitzer, K. A. (1977, January). *Magnetospheric magnetic field modeling* (Tech. Rep. No. Annual Report). Huntington Beach, CA.: McDonnell-Douglas Astronautics Co.

Ripoll, J. F., Chen, Y., Fennell, J. F., & Friedel, R. H. W. (2015, Jan). On long decays of electrons in the vicinity of the slot region observed by HEO3. *J. Geophys. Res.*, *120*(1), 460-478. doi: 10.1002/2014JA020449

Roberts, C. S. (1969, Jan). Pitch-angle diffusion of electrons in the magnetosphere. *Rev. Geophys.*, *7*, 305-337. doi: 10.1029/RG007i001p00305

Seki, K., Miyoshi, Y., Summers, D., & Meredith, N. P. (2005, Feb). Comparative study of outer-zone relativistic electrons observed by Akebono and CRRES. *J. Geophys. Res.*, *110*(A2), A02203. doi: 10.1029/2004JA010655

Selesnick, R. S., Su, Y.-J., & Sauvaud, J.-A. (2019). Energetic electrons below the inner radiation belt. *J. Geophys. Res.*, *124*(7), 5421-5440. doi: 10.1029/2019JA026718

Su, Y.-J., Johnston, W. R., Albert, J. M., Ginet, G. P., Starks, M. J., & Roth, C. J. (2012, Aug). SCATHA measurements of electron decay times at $5 < L \leq 8$. *J. Geophys. Res.*, *117*(A8), A08212. doi: 10.1029/2012JA017685

Vampola, A. L. (1971). Natural variations in the geomagnetically trapped electron population. In E. A. Warman (Ed.), *Proceedings of the National Symposium on Natural and Manmade Radiation in Space* (p. 539-547).

West, J., H. I., Buck, R. M., & Davidson, G. T. (1981, Apr). The dynamics of energetic electrons in the earth's outer radiation belt during 1968 as observed by the Lawrence Livermore National Laboratory's spectrometer on Ogo 5. *J. Geophys. Res.*, *86*(A4), 2111-2142. doi: 10.1029/JA086iA04p02111